NIH Public Access
Author Manuscript
J Phys Chem B. Author manuscript; available in PMC 2014 June 20.

Published in final edited form as:
J Phys Chem B. 2013 June 20; 117(24): 7345–7351. doi:10.1021/jp402270e.

Probing the Structure and Dynamics of Confined Water in AOT Reverse Micelles

Anna Victoria Martinez[†], **Laura Dominguez**[†], **Edyta Małolepsza**[†], **Adam Moser**[†,‡], **Zack Ziegler**[†], and **John E. Straub**[*,†]
Department of Chemistry, Boston, MA 02215, USA

Abstract

Reverse micelles are attractive nanoscale systems used for the confinement of molecules in studies of structure and chemical reactions, including protein folding and aggregation. The simulation of reverse micelles, in which a water "pool" is separated from a non-polar bulk phase by a surfactant layer, poses significant challenges to empirical force fields due to the diversity of interactions between non-polar, polar, and charged groups. We have explored the dependence of system density, reverse micelle structure, and water configurational relaxation times as a function of reverse micelle composition, including water:surfactant ratio, absolute number of water molecules, and force field using molecular dynamics simulations. The resulting structures and dynamics are found to depend more on the force field used than on varying interpretations of the water:surfactant ratio in terms of absolute size of the reverse micelle. Substantial deviations from spherical reverse micelle geometries are observed in all unrestrained simulations. Rotational anisotropy decay times and water residence times show a strong dependence of force field and water model used, but power-law relaxation in time is observed independent of the force field. Our results suggest the need for further experimental study of reverse micelles that can provide insight into the distribution and dynamics of shape fluctuations in these complex systems.

Keywords

reverse micelle composition; water dynamics; power-law relaxation

Introduction

Reverse micelles (RMs) have been the subject of experimental studies since the early 1940s.[1] Reverse micelles allow for a tunable amount of water to be encapsulated within a membrane like environment. The water cores of RMs have been found to behave similarly to cavities found in biological systems,[2] where the water-surfactant interface of reverse micelles mimics that behavior in a less complex environment and on a smaller scale.[3] These properties make RMs powerful tools in which to probe confinement effects and dehydration on biological molecules.[4–6]

Sodium bis(2-ethylhexyl) sulfosuccinate (AOT) is a commonly used surfactant as it readily forms RMs in non-polar solvents without a co-surfactant. AOT's branched structure allows

[*]To whom correspondence should be addressed: straub@bu.edu.
[†]Boston University
[‡]Current address: Loras College, Department of Chemistry, Dubuque, IA 52001, USA.

Supporting Information Available
Further analysis of the GROMOS systems including some comparison between the CHARMM and GROMOS force fields is reported in the Supporting Information. This material is available free of charge via the Internet at http://pubs.acs.org/.

NIH-PA Author Manuscript
NIH-PA Author Manuscript
NIH-PA Author Manuscript

NIH-PA Author Manuscript

NIH-PA Author Manuscript

NIH-PA Author Manuscript

the molecules to pack together and dissolve large amounts of water.[7,8] The shape, size and composition of RMs have been studied using many experimental techniques including NMR,[9] small angle X-ray scattering (SAXS),[10] dynamic light scattering (DLS),[11] and pulsed gradient stimulated echo.[12] The size of reverse micelles depends in part on their water loading (w_0), which is the ratio of water molecules to surfactant molecules:[13]

$$w_0 = \frac{[H_2O]}{[surfactant]}$$

The absolute composition of reverse micelles is still a matter of debate. The two most used estimates come from Amararene *et al.*[10] using SAXS and volumetric measurements and Eicke *et al.*[11] using analytic ultracentrifuge. These estimates disagree by as much as 35% for low water loadings (w_0 = 3–10), and the Waks work reports very small molecular water volumes for these. Further, the shape of AOT RMs is also still in question.[14]

Significant computational work has been performed using AOT RMs.[15–25] Some earlier simulations employed implicit solvent models in which the surfactant head groups were represented by a single charge interaction site, the water was treated explicitly, and a continuum potential was used to represent the non-polar solvent and the surfactant tail groups.[15–17] While useful, the implicit solvent model employed in that pioneering work failed to provide structural information for the surfactant or the interaction between the surfactant and the non-polar solvent. These simulations also spherically constrained the water core of the RM, not taking into account any deformation in shape or water penetration into the surfactant region of the RM.

To obtain more detailed structural information about reverse micelles, Abel *et al.* ran the first all atom simulations of AOT RMs of w_0 = 3, 5 and 7 in isooctane. They observed that within a few hundred picoseconds the RMs deviated from their original spherical shape and became elliptical as in the coarse grained RM simulations. The properties of water also became more bulk-like as the RMs increased in size. This work led to the first insights into the nature of the equilibrium structural ensemble of AOT RMs.[18]

Brodskaya *et al.* developed a coarse-grained model for AOT surfactant in hexane. They simulated RMs of w_0 = 2, 3, 4 and 5 and studied the effects of size and water content on structure.[19] In their 2-ns simulations the RMs, which were initially spherical, evolved into elliptical shapes. The change in shape was less pronounced as the RMs increased in size.[20] They also studied the translational diffusion within the reverse micelles and found that mobility of ions, polar heads of AOT, and water increased as the RMs increased in size.[21] Using a united atom model Chowdhary and Ladanyi simulated AOT RMs (w_0 = 2 – 7.5) in isooctane and examined the effect of RM size on structure.[22]

Tian and Garcia performed landmark simulations of the self-assembly of RMs [23] for compositions relevant to w_0 = 6 and 11. The simulated dynamics were extensive, showing the formation of small RMs and RM fusion ultimately forming RMs of an elliptical structure.

Graeve *et al.* performed experimental and computational studies (including self-assembly) investigating the size and shape of AOT RMs. In their initial work they observed significant deviations from the initial spherical shape for small RMs within the 1 ns of simulation time. They also noted that there is less fluctuation in shape for the larger RMs (w_0 > 10).[24] In a subsequent extensive and critical study of RM structure, they compared the results of their computational work to dynamic light scattering experiments on the same systems. They

NIH-PA Author Manuscript

NIH-PA Author Manuscript

NIH-PA Author Manuscript

observed highly qualitative agreement between their simulations and experiment, and found nonspherical shapes for the reverse micelles.[25]

Because previous theoretical work has generally employed spherical restraints, focused on a single w_0, used a single absolute composition estimate, or used a single force field, this work broadens the understanding of how these choices affect AOT RM simulations. In this work we used two force fields to simulate 12 reverse micelle systems (four spherically restrained, eight unrestrained) of w_0 = 6 and 10 using both experimental composition estimates. The compositions of the reverse micelles systems are outlined in Table 1.

Methods

RM systems were generated using the CHARMM32 package with the CHARMM27 all atom force field for proteins and lipids and the TIP3P water model for CHARMM.[26] CHARMM parameters for AOT and isooctane were taken from the work of of Abel *et al.*[18] For the spherically restrained RMs a massless dummy atom was fixed in the center of the RM. A harmonic restraint of 2 kcal/mol/Å was placed on the sulfur atom of each AOT molecule to keep it within a certain distance of the dummy atom (see Table 1). The distance restraints were chosen to agree with experimental measurements of the solution density in Ref. [10] and [11].

The starting structures for the unrestrained RMs were used for the GROMOS systems which were generated with the GROMOS96 53a6 united atom force field.[27] As there is no previous work in the literature modeling AOT with this force field, we attempted to remain as “force field consistent” as possible in using GROMOS to generate the AOT head group parameters. The parameters for the sulfur head group began with a choice of the sulfur parameters used for DMSO.

NAMD[28] and GROMACS were used for the production runs of the CHARMM and GROMOS systems respectively. The cutoff for the short-range electrostatics calculations was set to be 12 Å, and Ewald was used for the long-range electrostatics. The temperature was held constant at 300 K, and the pressure was held constant at 1 atm using the Langevin[29,30] (for NAMD) and Berendsen[31] (for GROMACS) pistons. There are alternatives based on extended-Lagrangian methods, such as a combination of Nose-Hoover chains with an Anderson piston, that are more elegant. However, we have not observed thermostat-dependent differences in the results for dynamics or equilibrium averaging for systems of the size studied in this work. SHAKE was used to keep bonds containing hydrogen atoms rigid. Each trajectory was run for 25 ns saving data every 0.1 ps. Analysis of all systems was performed using CHARMM, GROMACS and MDAnalysis.[32]

Results

Agreement between simulated and observed densities

Experimentally the density of the w_0 = 6 RMs is observed to be higher than the density of the w_0 = 10 RMs.[10] The values we report for the unrestrained CHARMM RMs in Figure 1 follow this trend. For the density calculations we used CHARMM to calculate the volume and density of a water box to determine appropriate values for probe radius and grid spacing, which were then used to calculate the volumes and densities for the reverse micelle systems. In all cases, the Eicke composition leads to a lower density than the Waks composition. While our simulated densities may be higher or lower than experimental values, are all within approximately 5% of these values, regardless of composition or force field (for GROMOS data see Supporting Information). The densities of the spherically

NIH-PA Author Manuscript

NIH-PA Author Manuscript

NIH-PA Author Manuscript

restrained RMs are higher than for the unrestrained RMs, but are still within 2% of the experimental values.

Unrestrained RMs are not spherical

The initial geometry of all simulated reverse micelles was spherical. In contrast to the shape of the spherically restrained RMs, the shape of the unrestrained RMs changed significantly. The unrestrained CHARMM RMs evolved from spheres to a rod-like shapes, and the unrestrained GROMOS RMs became disc- and donut-like. To quantify the changes in geometry we calculated several shape parameters including the moments of inertia, the semi-axes, and the eccentricity of each RM. The moments of inertia I_1, I_2, I_3 for an ellipse with semi-axes *a*, *b*, *c* are

$$I_1=\frac{m}{5}(b^2+c^2)$$
$$I_2=\frac{m}{5}(c^2+a^2)$$
$$I_3=\frac{m}{5}(a^2+b^2)$$

For spherical objects, $I_1 \approx I_2 \approx I_3$ and $a \approx b \approx c$. For a prolate ellipsoid (or a rod), $I_1 \approx I_2 > I_3$, and $a \approx b < c$. For an oblate ellipsoid (or a disc) $I_1 \approx I_2 < I_3$, and $a \approx b > c$. The eccentricity, *e*, of a shape is given by

$$e=\sqrt{1-\frac{c^2}{a^2}}$$

where *e* is zero for a perfect sphere and $e \rightarrow 1$ for disc- and rod-like shapes.[18]

Table 2 shows the average moments of inertia, the semi-axes, and the eccentricity for each of the CHARMM unrestrained RMs for the last 15 ns of simulation. The differences in the values of I_1, I_2, and I_3 and *a*, *b*, and *c* indicate non-spherical shapes. The moments of inertia for the CHARMM systems fluctuated significantly tending towards two large moments and one smaller one. The semi-axes also fluctuated, tending towards two short semi-axes and one long semi-axis, indicating a rod-like shape for these systems. The moments of inertia and the semi-axes for the GROMOS systems fluctuated generally indicating that the RMs shifted from spheres to disc-like shapes.

The eccentricity for all systems increased with time representing the shape evolution away from spherical. Figure 2 shows the eccentricity parameter for the CHARMM unrestrained RMs from 10 to 25 ns along with the distribution of eccentricity values for each RM. For the restrained RMs, there was little fluctuation for all values (data not shown). Figure 3 shows images of the unrestrained RMs for the CHARMM force field at 0, 15 and 25 ns following initial “equilibration.” GROMOS data is available in the Supporting Information.

Based on these results the shape of the RMs is more dependent on force field than composition. One main difference between the two force fields is the partial charges on the atoms. The CHARMM force field assigns a non-zero partial charge to every atom.[26] The AOT and isooctane parameters of Abel *et al.* follow this pattern.[18] In the GROMOS force field not every atom has a non-zero partial charge.[27] For AOT molecules the only atoms with non-zero partial charges are the sulfur, the oxygens, and the ester carbons. The rest of the aliphatic carbons have partial charges of zero. Because of the lack of partial charges in the GROMOS parameters there are no coulombic interactions between the water molecules

NIH-PA Author Manuscript

NIH-PA Author Manuscript

NIH-PA Author Manuscript

and the AOT tails, which apparently leads to a stabilization in the geometry of the reverse micelles. In the CHARMM systems the waters interact more strongly with the AOT head groups and hydrate the aliphatic tails to some extent. Water observed to penetrate the surfactant layer allows the shape of the RMs to be more flexible.

Water relaxation shows highly non-exponential behavior

The rotational anisotropy correlation function can be calculated by taking the dot product of the unit vectors, $\hat{u}$, in the direction of the O-H bonds, and then calculating the the correlation function of the second Legendre polynomial, P_2, as

$$C_2(t)=\langle P_2(\hat{u}(t)\cdot\hat{u}(0))\rangle$$

where $P_2(x) = (3x^2-1)/2$ and $x = \cos\theta = (\hat{u}(t)\cdot\hat{u}(0))$.[33] The second Legendre polynomial is relevant as it is used in analyzing order of liquid crystals.[34] The limit of $\langle P_2(x)\rangle \rightarrow 0$ indicates a random, isotropic system with fast decay times and $\langle P_2(x)\rangle \rightarrow 1$ indicates a more ordered system with slow decay times.[34]

The second-rank rotational anisotropy decay auto-correlation function (ACF) of the water was computed and compared to experimental values.[35] The rotational anisotropy decay ACF provides insight on restrictions in structural dynamics of water in confined areas, such as RMs of $w_0 < 20$. Experiments show that confined water rotates slowly and has a long rotational anisotropy decay time.[36] Rotational anisotropy decay times for water in reverse micelles may be extracted by fitting the ACFs to exponential functions.[35–37] The rotational anisotropy decay of bulk water and water in large RMs ($w_0 = 20, 40, 60$) can be fit to a single exponential function. The rotational anisotropy decay of water in small RMs ($w_0 < 20$) is not observed to decay as a single exponential, with confined water exhibiting multiple[38] or stretched exponential[35] behavior and multiple relaxation times on short time scales (~10–20 ps), and power law decay on longer time scales.[39–41] Piletic *et al.* found that for RMs of $w_0 \leq 10$, the water orientational relaxation behaved bi-exponentially with long decay times of 50, 30 and 18 ps and short decay times of 0.9, 1.0, and 1.5 ps for RMs of $w_0 = 2, 5$, and 10 respectively.[36]

We calculated the rotational anisotropy auto-correlation functions for the last 2000 ps of our simulations averaging over 1000 ps windows. For short time periods (~20 ps), the water rotational anisotropy relaxation in our simulations can be described either by using a sum of three exponential functions[38,42] or a stretched exponential function.[40,41,43] While the stretched exponential function does provide a good fit to short time data, an intuitively appealing approach employs a sum of exponentials where “types of water” are identified in the system with each “type” being associated with a particular mean relaxation time. Examples include studies of reverse micelles[38] and studies of water at the lipid-water interface[42] that suggest the water dynamics are best described by a sum of three exponentials. Biswas *et al.* proposed a tri-exponential model in which the rotational anisotropy decay times were calculated for three layers of water – a surface layer, an intermediate layer and a central layer. Each layer exhibited tri-exponential behavior, with the surface layer having the slowest decay times and the intermediate layer having the fastest decay times.[38]

Figure 4 shows the rotational anisotropy ACFs with tri-exponential fits (top) and stretched exponential fits (bottom) for the unrestrained CHARMM RMs. The plots show that the ACFs fit well to tri-exponential ($C_0e^{-x/\tau_0} + C_1e^{-x/\tau_1} + C_2e^{-x/\tau_2}$) or stretched exponential ($e^{-(x/\tau)^\beta}$) functions up to ~20 ps, but these functions fail to capture the longer decay time

NIH-PA Author Manuscript

NIH-PA Author Manuscript

NIH-PA Author Manuscript

features of the ACF. For the stretched exponential fits we obtained τ values ranging from 0.61 ps to 0.85 ps and β values between 0.42 and 0.5 for the restrained and unrestrained CHARMM RMs. Pieniazek *et al.*[35] obtained β values ranging from 0.17 to 0.37, which is indicative of collective behavior for the water. The β values they report are for RMs of w_0 = 2, 4 and 7.5. In smaller RMs, water dynamics will be more collective which may explain the difference in our values. While the GROMOS rotational anisotropy decay times are much slower, tri-exponential functions also fit the first 20 ps of the ACFs, but fail to describe the longer decay times. Further analysis is provided in the Supporting Information.

For longer time periods of up to approximately 1000 ps, the stretched exponential model fails to capture the water dynamics. Data from our CHARMM simulations are better described by a pair of power laws of the form t^{-b1} and t^{-b2} where the b_1 component fits longer decay times and the b_2 component fits shorter decay times. In Figure 5 the rotational anisotropy ACFs along with the power law fits are plotted on a log-log plot. The figure shows that the ACFs fit well to a power law t^{-b1} after ~1 ps with b_1 values between 0.8 and 1.1. A second power law t^{-b2} (not shown on graph) describes the short times up to 1 ps with b_2 values between 0.33 and 0.4. As the reverse micelles increase in size, the behavior of the water approaches that of bulk.

Several other groups have analyzed the rotational anisotropy decay of water in confined environments other than reverse micelles.[39–41,43–45] They find that while the initial decay (up to 10 or 20 ps) can be characterized well with a stretched exponential or sum of exponential functions, the longer decay times are described more accurately by a power law or a pair of power laws.

Our observation of power-law relaxation of the rotational anisotropy decay for water in reverse micelles is consistent with observations by Laage and Thompson in their computational work on water confined in silica pores,[39] and experimental work by Scodinu *et al.*[44] and Farrer *et al.*[45] using optical Kerr effect spectroscopy to study orientational dynamics of confined water. Our data for the rotational anisotropy decay times for the SPC water in the GROMOS simulations show slower decay times but are consistent with the observation that multiple or stretched exponential functions are not able to capture the relaxation behavior past 20 ps.

In addition to the rotational anisotropy decay, we calculated the residence times of the water molecules with respect to each AOT in the unrestrained RMs for the last 2000 ps. We defined residence time to be the length of time an individual water molecule remained within 4 Å of an AOT head group oxygen. The distributions of the residence times for the unrestrained CHARMM and GROMOS systems are shown on a log-log plot in Figure 6. The residence time distributions, like the rotational anisotropy, decay as power laws. The CHARMM data is fit well by two power laws and the GROMOS to one. This graph shows that in general the TIP3P water has shorter residence times than SPC water. The GROMOS simulations have a larger fraction of waters with residence times of 100 ps or longer which may contribute to the long rotational anisotropy decay times.

Discussion

Previous RM simulations by Ladanyi *et al.*,[22] which used the Eicke composition, resulted in more spherical RMs than what we present here. We believe this difference results from the force field used. It is important to note that each of our simulations was performed using parameters specifically for each force field used. In Ladanyi's model, parameters from more than one force field were used,[22] which may be partially responsible for the observed differences.[46] The AOT parameters are similar to those in the GROMOS force field, with

NIH-PA Author Manuscript

NIH-PA Author Manuscript

NIH-PA Author Manuscript

non-zero partial charges on the oxygens and ester carbons but partial charges of zero on the sulfur atom and the remaining aliphatic carbons. The isooctane carbons also have partial charges of zero. This means there are only electrostatic and coulombic interactions between the water and the AOT head group region. This appears to lead to the lack of water penetration to the AOT tails with the majority of the waters remaining in the core of the RM. Two additional simulations of the Waks w_0 = 6 RM were performed using CHARMM and GROMOS. In the CHARMM simulations we changed the partial charges of the AOT and the isooctane to be the same as those used in Ladanyi's simulations and in the GROMOS simulations we changed the water from SPC to SPC/E. These changes had no significant effects on the shapes of the RMs.

Simulations by Graeve *et al.*[24,25] resulted in reverse micelles with cylindrical or elongated donut-like shapes. The type and range of shape fluctuations in our simulations are consistent with those of Graeve and coworkers, which was also consistent with the results of their experimental light scattering studies.[25]

Their work employed the same force field and parameters for AOT as in the CHARMM simulations presented in this work. They studied RMs of various w_0 by keeping the number of AOT molecules constant and varying the amount of water present. They note that the absolute composition of the RMs is less important than the water:surfactant ratio as their simulation results are in good agreement with their experimental studies of the same systems indicating non-spherical RMs.

Conclusion

Reverse micelles are widely used in experimental studies of molecular structure and dynamics, including protein folding and aggregation, using NMR and optical spectroscopies.[9–11] Due to the complexity of interactions between the sequestered molecules and the surrounding water pool and surfactant, simulation studies are essential to the complete interpretation of experimental spectroscopic studies of the structure. We have used two force fields to simulate reverse micelles based on two alternative interpretations of the water loading in terms of the absolute numbers of water and surfactant molecules determined by two experimental groups.[10,11] We find the properties of the RMs to be more dependent on the size (w_0 = 6 vs. 10) and the force field used than the absolute composition. Within each force field both compositions yielded similar densities close to the experimental values. The simulated rotational anisotropy decay times for the water were on the same order of magnitude for the w_0 values in each force field. The simulations of spherically restrained systems were used to provide a "control," with which, for example, we could establish that water dynamics in the restrained RMs are similar to water dynamics in the unrestrained RMs in which the waters/surfactant interface is structurally distinct. Shape parameters calculated from the moments of inertia also yielded comparable results indicating rod-like shapes for the CHARMM systems and disc- or donut-like shapes for the GROMOS systems.

There exist substantial differences in the interpretation of reverse micelle structure and dynamics in the literature.[6,18,22,24,25] Most simulation studies support the conclusion that there are significant shape fluctuations, away from the idealized spherical geometry, that are important to the overall system energetics and dynamics.[18,23,47] However, many experimental studies are interpreted with the assumption of an idealized spherical geometry of the reverse micelle and internal water pool.[5,7,48,49] Moreover, simulation studies indicate a broad distribution of relaxation times for water rotational anisotropy, with significant force field dependence. Further experimental studies of both the structure and dynamics of reverse

NIH-PA Author Manuscript

NIH-PA Author Manuscript

NIH-PA Author Manuscript

micelle systems are needed to clarify the nature of reverse micelle structure and to evaluate critically the predictions of simulation models.

Supplementary Material

Refer to Web version on PubMed Central for supplementary material.

Acknowledgments

The authors gratefully acknowledge the support of a grant from the National Institutes of Health (RO1 GM076688), the resources of the Center for Computational Science at Boston University, the Schlumberger Foundation Faculty for the Future Program and CONACYT. This work used the Extreme Science and Engineering Discovery Environment (XSEDE), which is supported by National Science Foundation grant number OCI-1053575.

References

1. Hoar T, Schulman J. Transparent Water-in-Oil Dispersions: The Oleopathic Hydro-Micelle. Nature. 1943; 152:102–103.
2. Levinger NE. Water in Confinement. Science. 2002; 298:1722–1723. [PubMed: 12459570]
3. Thompson KF, Gierasch LM. Conformation of a Peptide Solubilizate in a Reversed Micelle Water Pool. J Am Chem Soc. 1984; 106:3648–3652.
4. Mukherjee S, Chowdhury P, Gai F. Tuning the Cooperativity of the Helix-Coil Transition by Aqueous Reverse Micelles. J Phys Chem B. 2006; 110:11615–11619. [PubMed: 16800453]
5. Mukherjee S, Chowdhury P, Gai F. Effect of Dehydration on the Aggregation Kinetics of Two Amyloid Peptides. J Phys Chem B. 2009; 113:531–535. [PubMed: 19132862]
6. Martinez AV, DeSensi SC, Dominguez L, Rivera E, Straub JE. Protein Folding in a Reverse Micelle Environment: The Role of Confinement and Dehydration. J Chem Phys. 2011; 134:055107. [PubMed: 21303167]
7. De TK, Maitra A. Solution Behaviour of Aerosol OT in Non-Polar Solvents. Adv Colloid Interface Sci. 1995; 59:95–193.
8. Nave S, Eastoe J, Heenan RK, Steytler D, Grillo I. What Is So Special about Aerosol-OT? 2 Microemulsion Systems. Langmuir. 2000; 16:8741–8748.
9. Maitra A. Determination of Size Parameters of Water-Aerosol OT-Oil Reverse Micelles from Their Nuclear Magnetic Resonance Data. J Phys Chem. 1984; 88:5122–5125.
10. Amararene A, Gindre M, Huérou JYL, Urbach W, Valdez D, Waks M. Adiabatic Compressibility of AOT Sodium Bis2-ethylhexylsulfosuccinate Reverse Micelles: Analysis of a Simple Model Based on Micellar Size and Volumetric Measurements. Phys Rev E. 2000; 61:682–689.
11. Eicke HF, Rehak J. On the Formation of Water/Oil-Microemulsions. Helv Chem Acta. 1976; 59:2883–2891.
12. Law SJ, Britton MM. Sizing of Reverse Micelles in Microemulsions using NMR Measurements of Diffusion. Langmuir. 2012; 28:11699–11706. [PubMed: 22794150]
13. Hauser H, Haering G, Pande A, Luisi P. Interaction of Water with Sodium Bis(2-ethyl-1-hexyl) Sulfosuccinate in Reversed Micelles). J Phys Chem. 1989; 93:7869–7876.
14. Levinger NE, Swafford LA. Ultrafast Dynamics in Reverse Micelles. Annu Rev Phys Chem. 2009; 60:385–406. [PubMed: 18999990]
15. Faeder J, Ladanyi BM. Molecular Dynamics Simulations of the Interior of Aqueous Reverse Micelles. J Phys Chem B. 2000; 104:1033–1046.
16. Faeder J, Ladanyi BM. Solvations Dynamics in Aqueous Reverse Micelles: A Computer Simulations Study. J Phys Chem B. 2001; 105:11148–11158.
17. Faeder J, Ladayni BM. Solvation Dynamics in Reverse Micelles: The Role of Headgroup-Solute Interactions. J Phys Chem B. 2005; 109:6732–6740. [PubMed: 16851757]
18. Abel S, Sterpone F, Bandyopadhyay S, Marchi M. Molecular Modeling and Simulations of AOT-Water Reverse Micelles in Isooctane: Structural and Dynamic Properties. J Phys Chem B. 2004; 108:19458–19466.

NIH-PA Author Manuscript

NIH-PA Author Manuscript

NIH-PA Author Manuscript

19. Mudzhikova G, Brodskaya E. Molecular Simulation of an Aerosol OT Reverse Micelle: 1. The Shape and Structure of a Micelle. Colloid J. 2006; 68:729–737.
20. Brodskaya EN, Mudzhikova GV. Molecular Dynamics Simulation of AOT Reverse Micelles. Mol Phys. 2006; 104:3635–3645.
21. Mudzhikova G, Brodskaya E. Molecular Simulation of an Aersol OT Reverse Micelle: 2. Energy and Kinetic Characteristics. Colloid J. 2006; 68:738–742.
22. Chowdhary J, Ladanyi BM. Molecular Dynamics Simulation of Aerosol-OT Reverse Micelles. J Phys Chem B. 2009; 113:15029–15039. [PubMed: 19842706]
23. Tian J, Garcia AE. Simulations of the Confinement of Ubiquitin in Self-Assembled Reverse Micelles. J Chem Phys. 2011; 124:225101. [PubMed: 21682536]
24. Gardner A, Vásquez V, Clifton A, Graeve O. Molecular Dynamics Analysis of the AOT/Water/Isooctane System: Effect of Simulation Time, Initial Configuration, and Model Salts. Fluid Phase Equil. 2007; 262:264–270.
25. Vasquez VR, Williams BC, Graeve OA. Stability and Comparative Analysis of AOT/Water/Isooctane Reverse Micelle System Using Dynamic Light Scattering and Molecular Dynamics. J Phys Chem B. 2011; 115:2979–2987. [PubMed: 21384835]
26. MacKerell AD, Bashford D, Bellott M Jr, RLD, Evanseck JD, Field MJ, Fischer S, Gao J, Guo H, Ha S, Joseph-McCarthy D, Kuchnir L, Kuczera K, Lau FTK, Mattos C, Michnick S, Ngo T, Nguyen DT, Prodhom B III, WER, Roux B, Schlenkrich M, Smith JC, Stote R, Straub JE, Watanabe M, Wiórkiewicz-Kuczera J, Yin D, Karplus M. All-Atom Empirical Potential for Molecular Modeling and Dynamics Studies of Proteins. J Phys Chem B. 1998; 102:3586–3616.
27. Oostenbrink C, Villa A, Mark AE, van Gunsteren WF. A Biomolecular Force Field Based on the Free Enthalpy of Hydration and Solvation: The GROMOS Force-Field Parameter Sets 53A5 and 53A6. J Comput Chem. 2004; 25:1656–1676. [PubMed: 15264259]
28. Phillips JC, Braun R, Wang W, Gumbart J, Tajkhorshid E, Villa E, Chipot C, Skeel RD, Kaleé L, Schulten K. Scalable Molecular Dynamics with NAMD. J Comput Chem. 2005; 26:1781–1802. [PubMed: 16222654]
29. Martyna GJ, Tobias DJ, Klein ML. Constant Pressure Molecular Dynamics Algorithms. J Chem Phys. 1994; 101:4177–4189.
30. Feller SE, Zhang Y, Pastor RW, Brooks BR. Constant Pressure Molecular Dynamics Simulation: The Langevin Piston Method. J Phys Chem. 1995; 103:4613–4621.
31. Berendsen H, Postma J, van Gunsteren W, DiNola A, Haak J. Molecular Dynamics with Coupling to an External Bath. J Chem Phys. 1984; 81:3684–3690.
32. Michaud-Agrawal N, Denning EJ, Woolf TB, Beckstein O. Software News and Updates MDAnalysis: A Toolkit for the Analysis of Molecular Dynamics Simulations. J Comput Chem. 2011; 32:2319–2327.
33. Impey R, Madden P, McDonald I. Spectroscopic and Transport Properties of Water. Mol Phys. 1982; 46:513–539.
34. Ghosh S. A Model for the Orientational Order in Liquid Crystals. Il Nuovo Cimento. 1984; 4:229–244.
35. Pieniazek PA, Lin YS, Chowdhary J, Ladanyi BM, Skinner JL. Vibrational Spectroscopy and Dynamics of Water Confined inside Reverse Micelles. J Phys Chem B. 2009; 113:15017–15028. [PubMed: 19842648]
36. Piletic IR, Moilanen DE, Spry D, Levinger NE, Fayer M. Testing the Core/Shell Model of Nanoconfined Water in Reverse Micelles Using Linear and Nonlinear IR Spectroscopy. J Phys Chem A. 2006; 110:4985–4999. [PubMed: 16610816]
37. Fayer MD. Dynamics of Water Interacting with Interfaces, Molecules, and Ions. Acc Chem Res. 2012; 45:3–14. [PubMed: 21417263]
38. Biswas R, Chakraborti T, Bagchi B, Ayappa K. Non-Monotonic, Distance Dependent Relaxation of Water in Reverse Micelles: Propagation of Surface Induced Frustration Along Hydrogen Bond Networks. J Chem Phys. 2012; 137:014515. [PubMed: 22779673]
39. Laage D, Thompson WH. Reorientation Dynamics of Nanoconfined Water: Power-Law Decay Hydrogen-Bond Jumps, and a Test of a Two-State Model. J Chem Phys. 2012; 136:044513. [PubMed: 22299897]

NIH-PA Author Manuscript

NIH-PA Author Manuscript

NIH-PA Author Manuscript

40. Marchi M, Sterpone F, Ceccarelli M. Water Rotational Relaxation and Diffucion in Hydrated Lysozyme. J Am Chem Soc. 2002; 124:6786–6791.

41. Pizzitutti F, Marchi M, Sterpone F, Rossky PJ. How Protein Surfaces Induce Anomalous Dynamics of Hydration Water. J Phys Chem B. 2007; 111:7584–7590. [PubMed: 17564431]

42. Lu W, Kim J, Qiu W, Zhong D. Femtosecond Studies of Tryptophan Solvation: Correlation Function and Water Dynamics at Lipid Surfaces. Chem Phys Lett. 2004; 388:120–126.

43. Johnston D. Stretched Exponential Relaxation Arising From a Continuous Sum of Exponential Decays. Phys Rev B. 2006; 74:184430.

44. Scodinu A, Fourkas JT. Comparison of the Orientational Dynamics of Water Confined in Hydrophobic and Hydrophili Nanopors. J Phys Chem B. 2002; 106:10292–10295.

45. Farrer RA, Fourkas JT. Orientational Dynamics if Liquids Confined in Nanoporous Sol-Gel Glasses Studied by Optical Kerr Effect Spectroscopy. Acc Chem Res. 2003; 36:605–612. [PubMed: 12924957]

46. Pastor RW, MacKerell ADJ. Development of the CHARMM Force Field of Lipids. J Phys Chem Lett. 2011; 2:1526–1532. [PubMed: 21760975]

47. Tian J, Garcia AE. An Alpha-Helical Peptide in AOT Micelles Prefers to be Localized at the Water/Headgroup Interface. Biophys J. 2009; 96:57–59.

48. Kotlarchyk M, Huang JS. Structure of Reversed Micelles Determined by Small-Angle Neutron Scattering. J Phys Chem. 1985; 89:4382–4386.

49. Mukherjee S, Chowdhury P, Gai F. Infrared Study of the Effect of Hydation on the Amide I Band and Aggregation Properties of Helical Peptides. J Phys Chem B. 2007; 111:4596–4602. [PubMed: 17419612]

NIH-PA Author Manuscript

NIH-PA Author Manuscript

NIH-PA Author Manuscript

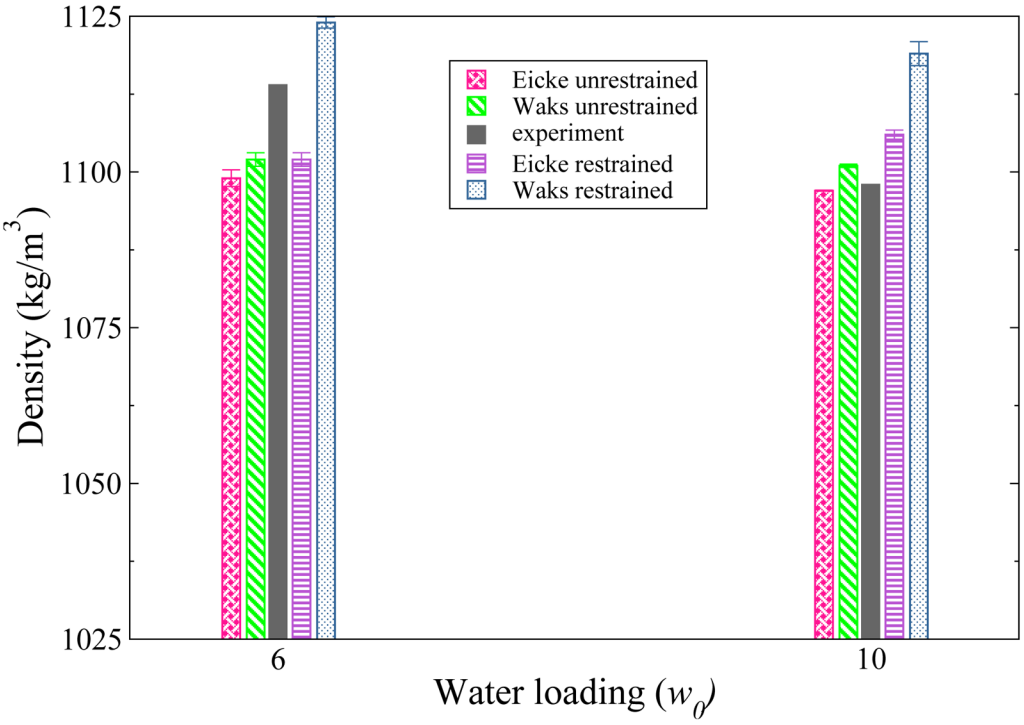

Figure 1.

Densities (kg/m^3) for all simulated CHARMM RMs. The experimental values are in dark gray. The densities for the unrestrained RMs are to the left of the experimental values, and the densities for the restrained RMs are to the right. All calculated values for the CHARMM simulations are within 2% of the reported experimental densities.

NIH-PA Author Manuscript

NIH-PA Author Manuscript

NIH-PA Author Manuscript

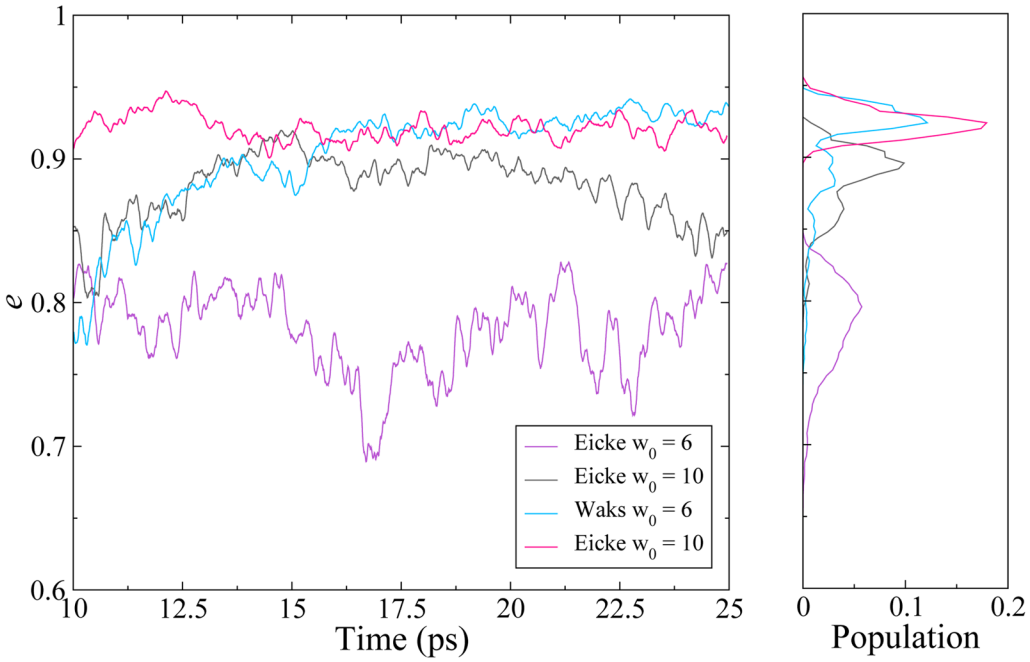

Figure 2.

Eccentricity parameter for the CHARMM unrestrained RMs for the last 15 ns of simulation. The eccentricity parameter is plotted versus time (left) with the normalized histogram of eccentricity values shown for the last 15 ns (right).

NIH-PA Author Manuscript

NIH-PA Author Manuscript

NIH-PA Author Manuscript

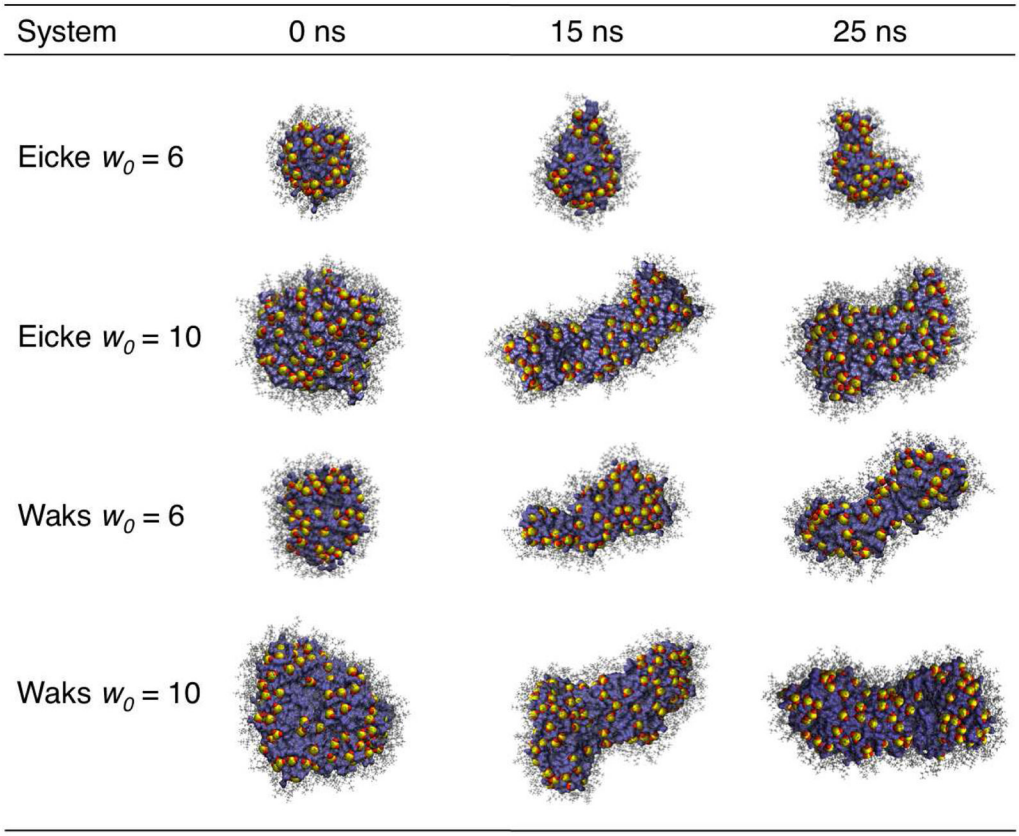

Figure 3.
Structures of the unrestrained reverse micelles for the CHARMM force field. The images from left to right show the structures of the RMs at 0, 15, and 25 ns. The AOT sulfur head groups are represented by yellow sulfur atoms and red oxygen atoms. The AOT tails are in gray, and the water is in blue.

NIH-PA Author Manuscript

NIH-PA Author Manuscript

NIH-PA Author Manuscript

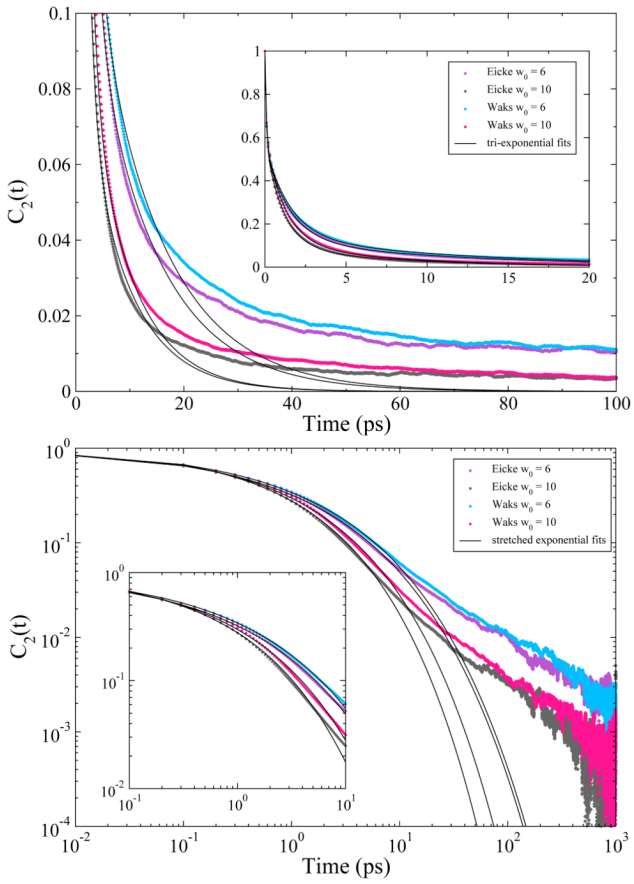

Figure 4.

Rotational anisotropy decay auto-correlation functions for the unrestrained CHARMM reverse micelles. The inset plots show that the auto-correlation functions fit well to a tri-exponential function (top) or a stretched exponential function (bottom) up to approximately 10 or 20 ps. The large plots show that these fits fails to describe the correlation functions on longer time scales.

NIH-PA Author Manuscript
NIH-PA Author Manuscript
NIH-PA Author Manuscript

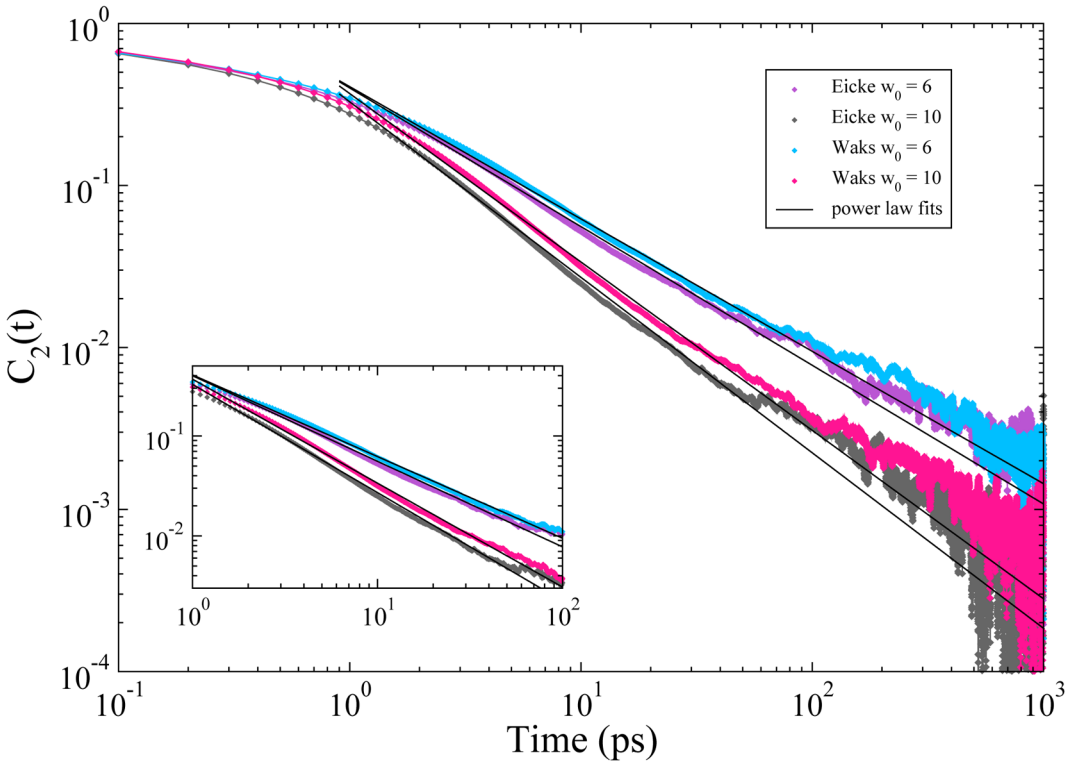

Figure 5.
Rotational anisotropy decay auto-correlation functions for the unrestrained CHARMM reverse micelles on a log-log scale. The plot shows that the auto-correlation functions are described well with a power law decay from 1 to 100ps.

NIH-PA Author Manuscript
NIH-PA Author Manuscript
NIH-PA Author Manuscript

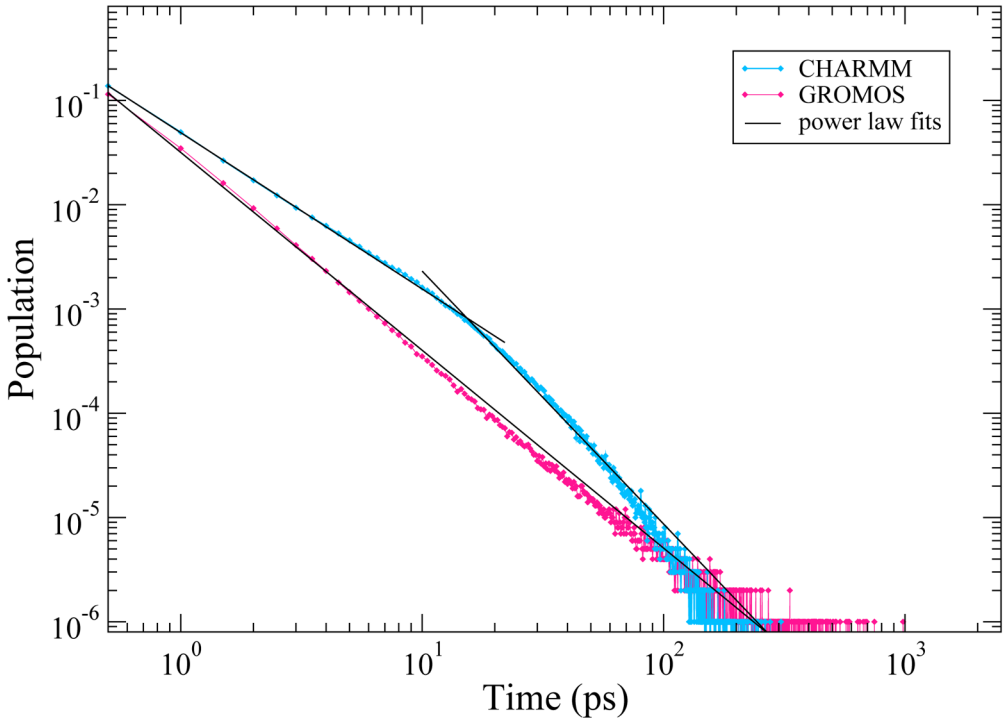

Figure 6.
Distribution of water residence time for all AOTs head groups in the unrestrained RMs.

NIH-PA Author Manuscript NIH-PA Author Manuscript NIH-PA Author Manuscript

Table 1

Reverse micelle compositions including the water loading (w_0), total number of AOT and water molecules (n_{AOT} and n_{H_2O}), the mole fraction of isooctane (χ_{ISO}), and the radius of the water pool for each system. The values given for the radii were the initial values for the unrestrained systems and the distance paramters placed on the spherically restrained systems throughout the simulations.

Composition	w_0	n_{AOT}	n_{H_2O}	χ_{ISO}	water radius (Å)
Eicke	6	50	300	0.81	12.00 – 16.00
Eicke	10	97	970	0.80	18.00 – 22.00
Waks	6	76	456	0.81	11.25 – 15.25
Waks	10	129	1290	0.83	18.00 – 22.00

J Phys Chem B. Author manuscript; available in PMC 2014 June 20.

NIH-PA Author Manuscript NIH-PA Author Manuscript NIH-PA Author Manuscript

Table 2

Average values for last 15 ns of simulation time for the moments of inertia I_1, I_2, I_3 (10^6 amu*Å^2), semiaxes *a*, *b*, *c* (Å^2), and eccentricity *e* for CHARMM unrestrained RM systems.

Composition	w_0	I_1	I_2	I_3	*a*	*b*	*c*	*e*
Unrestrained RMs - CHARMM force field								
Eicke	6	4.1 ± 0.2	5.1 ± 0.3	6.3 ± 0.2	25.8 ± 1.1	21.9 ± 0.9	16.1 ± 0.5	0.78 ± 0.03
Waks	6	6.4 ± 0.8	17.1 ± 2.0	18.4 ± 1.9	47.4 ± 2.3	18.6 ± 0.8	16.9 ± 0.6	0.93 ± 0.01
Eicke	10	12.2 ± 1.0	30.3 ± 2.9	31.7 ± 2.4	45.2 ± 2.8	23.6 ± 1.3	21.1 ± 0.9	0.88 ± 0.02
Waks	10	19.8 ± 1.0	55.8 ± 3.2	61.0 ± 2.3	54.8 ± 1.6	27.8 ± 1.6	21.2 ± 1.2	0.92 ± 0.01

J Phys Chem B. Author manuscript; available in PMC 2014 June 20.